Predictive large eddy simulations for urban flows : challenges and opportunities

Accepted Manuscript

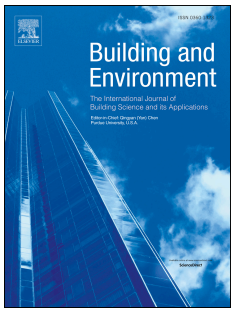

Predictive large eddy simulations for urban flows: Challenges and opportunities

C. García-Sánchez, J. van Beeck, C. Gorlé

PII: S0360-1323(18)30267-1

DOI: 10.1016/j.buildenv.2018.05.007

Reference: BAE 5445

To appear in: *Building and Environment*

Received Date: 4 February 2018

Revised Date: 7 April 2018

Accepted Date: 3 May 2018

Please cite this article as: García-Sánchez C, van Beeck J, Gorlé C, Predictive large eddy simulations for urban flows: Challenges and opportunities, *Building and Environment* (2018), doi: 10.1016/j.buildenv.2018.05.007.

Predictive Large Eddy Simulations for Urban Flows: Challenges and Opportunities

C. García-Sánchez[a,b,c,*], J. van Beeck[b], C. Gorlé[c]

[a] *EMAT, Department of Physics, University of Antwerp, Groenenborgerlaan 171, 2020 Antwerp, Belgium*
[b] *von Karman Institute for Fluid Dynamics, Waterloosesteenweg 72, 1640 Sint-Genesius-Rode, Belgium*
[c] *Department of Civil and Environmental Engineering, Stanford University, 473 Via Ortega, Stanford, CA 94305, USA*

Abstract

Computational fluid dynamics predictions of urban flow are subject to several sources of uncertainty, such as the definition of the inflow boundary conditions or the turbulence model. Compared to Reynolds-averaged Navier-Stokes (RANS) simulations, large eddy simulations (LES) can reduce turbulence model uncertainty by resolving the turbulence down to scales in the inertial subrange, but the presence of other uncertainties will not be reduced. The objective of this study is to present an initial investigation of the relative importance of these different types of uncertainties by comparing urban flow predictions obtained using RANS and LES to field measurements. The simulations are designed to reproduce measurements performed during the Joint Urban 2003 field experiments. The time-averaged velocity measured at an upstream wind sensor is used to define the inflow boundary condition, and the results are compared to time-averaged measurements at 34 locations

*Corresponding author
Email address: cgarcia-sanchez@carnegiescience.edu (C. García-Sánchez)

in the downtown area. For the turbulence kinetic energy, the LES is found to be more accurate than the RANS in 80% of the available high-frequency measurement locations. For the mean velocity field, this number reduces to 50% of all stations. Comparison of the LES results with a previous inflow uncertainty quantification study for RANS shows that locations where the LES is less accurate than the RANS correspond to locations where the RANS solution is highly sensitive to the inflow boundary conditions. This suggests that inflow uncertainties can be a dominant factor, and that their effect on LES results should be quantified to guarantee predictive capabilities.

Keywords: Large eddy simulations, uncertainty quantification, atmospheric boundary layer, urban wind flows.

1. Introduction

Considering the projected urban area population growth of 2.5 billion by 2050 [1], it is essential to design future cities for optimal air quality, human comfort, energy efficiency and resiliency. Wind flow predictions in urban canopies are relevant to a variety of sustainable urban design problems, including pedestrian wind comfort, pollutant dispersion, and urban wind energy harvesting. Improved wind forecasts using computational fluid dynamics (CFD) can support urban planners and policy makers to identify optimal design solutions and define best practice guidelines for sustainable cities.

However, CFD predictions of wind flow in urban environments present several challenges, primarily because it is not feasible to represent the full complexity of the urban flow phenomena in a numerical model. This results

in several sources of uncertainty in the simulations, ranging from uncertainties in the boundary conditions for the simulation to geometrical and physics model uncertainties. Given the high Reynolds number of urban flow problems, the turbulence model can be a significant source of physics model uncertainty. An important modeling choice is whether to perform Reynolds-averaged Navier-Stokes (RANS) simulations, where all the turbulent scales are modeled, or large-eddy simulations (LES), where the larger energy-containing scales are resolved and only the smaller scales are modeled. LES has the advantage of providing a higher-fidelity solution with considerably reduced uncertainties related to the turbulence model, but the high Reynolds number of atmospheric boundary layer (ABL) flows, on the order of 10^7, implies it is computationally expensive to resolve a sufficient portion of the turbulence spectrum. The turn-around time for the simulations increases from a few hours for RANS to several days or weeks for LES.

Several validation studies have compared the performance of RANS and LES to reproduce wind tunnel experiments of urban-type flows [2, 3, 4, 5, 6, 7, 8]. The general conclusion of these studies is that LES can provide considerably more accurate predictions than RANS. This indicates that the turbulence model is a dominant factor when predicting urban flow wind tunnel experiments. On the other hand, comparisons of LES to field measurements, which represent the full complexity of urban flows, are more scarce and reveal a more complex picture. Table 1 summarizes 6 published studies identified by the authors, including the type of comparison that was presented between the LES results and field measurement data.

LES study	Urban area	Type of comparison	Field compared
Hanna et al., 2006[9]	Manhattan	Qualitative contours	Wind
Patnaik et al. 2007[10]	Los Angeles	Congruency counts and mean	Scalar concentration
Dejoan et al., 2010[11]	MUST	Mean vertical profiles and fluctuating intensity	Scalar concentration
Neophytou et al., 2011[12]	JU2003	Mean values	Wind
Harms et al. 2011 [13]	JU2003	Instantaneous values	Peak concentration time
Nakayama et al., 2012[14]	Tokyo	Time series and gust factor	Wind

Table 1: Summary of LES studies comparing with field measurements in urban areas.

Hanna et al. [9] performed simulations over Manhattan, and presented a qualitative comparison of the results of 5 different CFD models and field data. While they retrieve the general flow patterns from the experiment, no conclusions on the quantitative predictive value of the simulations are provided. Nakayama et al. [14] used meteorological data as boundary conditions for LES simulations to reproduce a strong wind event occurring in downtown Tokyo during the passage of Typhoon Melor. A quantitative comparison of the velocity field indicates that the LES consistently over predicted horizontal wind speeds. Dejoan et al. [11] modeled the idealized configuration of the MUST experimental field campaign [15]. Their quantitative analysis focuses on the concentration field, and shows that changes in the inflow wind direction largely modify the dispersion patterns. This can be expected to complicate guaranteeing predictive capabilities for full-scale urban flows, were accurate definition of the inflow boundary conditions is a challenge. The studies by Patnaik et al. [10] and Harms et al. [13] consider validation of the FAST3D-CT MILES model, an LES model for urban scale flows, for prediction of puff dispersion field experiments in Los Angeles and in Oklahoma City respectively. They address the difficulties encountered due to

the sparsity of the experimental data in field experiments by constructing probability distributions from an ensemble of puff dispersion realizations to compare with the field data. The resulting probability distributions encompass the measured field data, which is an important step towards successful validation of the model and indicates the potential of using a statistical approach for validation with field experiments. Lastly, Neophytou et al. [12] also used LES to model the Joint Urban 2003 (JU2003) experiment, focusing on predictions of the mean velocity field. They compared a mass-consistent empirical diagnostic code, a RANS approach, and LES with field measurements in Oklahoma City, and found that the use of LES did not improve the comparison to the measurement data for the time-averaged velocity field. They mentioned a suboptimal simulation set-up for LES, together with the inherent uncertainty and natural variability in the wind field as reasons for a lack in improvement of the results.

The difficulties encountered in validation of LES with field experiments as opposed to validation with wind tunnel measurements indicate that the presence of additional uncertainties is an important outstanding challenge. The primary gain when using LES as opposed to RANS, is a reduction in the physics model uncertainty in the solution; the uncertainty in the definition of the boundary conditions or the geometry, which can be significant for urban flows, is not reduced. Since quantifying uncertainties in the boundary conditions inherently requires running a larger number of simulations [16, 17, 18], this quickly becomes intractable using LES. The challenge therefore becomes to balance the use of computational resources for reducing turbulence model form uncertainties, versus using them for quantifying other types of uncer-

tainties.

The objective of the present study is to further support the importance of striking this balance by comparing the predictive capabilities of LES to those of RANS for real urban flows. To achieve this we present a comparison of the performance of a single LES simulation and a single RANS simulation for predicting field measurements performed during the JU2003 field measurement campaign in downtown Oklahoma City. The results complement the previous work by Neophytou et al. [12] in several ways. First, the current LES set-up has been designed to identify if the lack of improvement previously observed could indeed be attributed to a suboptimal simulation set-up for the high-fidelity methodology. The computational mesh enables resolving the turbulence into the inertial sublayer, and the inflow boundary conditions realistically represent the neutral ABL flow at the time of the field experiment, with turbulent structures that are correlated in space and time. Second, the quantities of interest considered are both the mean velocity and the turbulence kinetic energy. In addition, turbulence spectra from the LES and the field experiment are compared to determine the capability of the LES to correctly predict the turbulence scales and their energy content. Third, the LES results are compared to the results obtained from a previous inflow uncertainty quantification (UQ) study, allowing to identify locations where the predictive capability of the LES might be hindered by the natural variability in the boundary conditions.

The remainder of this article is organized in six sections. Section 2 briefly introduces the JU2003 field measurement data used for validation [19]. Section 3 summarizes the set-up of the RANS simulations, including a short

description of the previously published inflow UQ study for this simulation [18]. Section 4 presents the governing equations and the computational and numerical set-up for the LES. Section 5 compares the RANS and LES results for the velocity and turbulence kinetic energy to the field measurement data. In addition, the results are interpreted in light of our previous RANS inflow UQ results. Section 6 summarizes the results and presents the conclusions.

2. Joint Urban 2003 experimental data

The JU2003 field measurement campaign was performed in Oklahoma city during the summer of 2003. The main purpose of the campaign was to provide quality-assured meteorological and tracer data sets for the validation of indoor and outdoor dispersion models in urban environments. Wind speeds, wind directions, and scalar concentrations were measured by sonic anemometers, airplane-based meteorological sensors, and fast-response tracer analyzers, respectively. The data also includes an accurate geometrical description; the geometrical complexity is related to the presence of buildings, since the state has a flat natural topography. The final data set provides a unique test case for full-scale validation of computational models of urban wind and dispersion.

The simulations are designed to reproduce the first half hour of Intensive Observation Period 9 (IOP9) from the experiment, which took place on the 27th of July from 04:00 to 04:30. This time period was selected for its near-neutral atmospheric conditions; it was also the focus of the previously published UQ study [18] that will be introduced in section 3 and used for comparison to the results in section 5. The objective is to evaluate the

capabilities of RANS and LES to predict the mean velocity field and the turbulence kinetic energy; for the LES we also consider a comparison of turbulence spectra. The wind flow measurements of interest to this validation effort were obtained by Dugway Proving Ground. Two different types of measurement stations were used: the portable weather information display system (P), and the super portable weather information display system (SP) [20]. Figure 1 shows the locations of both types of sensors.

Fifteen P stations were available during the experimental campaign. They measured the velocity magnitude and direction each second, and averaged the values over a 10 second interval before recording with a stated accuracy of $\pm 0.3 ms^{-1}$ and $\pm 3^{\circ}$. As can be observed in figure 1, the stations were located in downtown Oklahoma City at a height of 8m above ground level (with the exception of stations P14, located on a building roof, and P15, located at 30m height). Twenty SP stations were located in the downtown central business district, also at an average height of 8m. Each station measured with a sampling frequency of 10Hz, saving the data instantaneously for three velocity components with an accuracy corresponding to the highest value between $\pm 1\% rms$ and $\pm 0.05 ms^{-1}$. Some of these stations were placed next to P stations, such that their measurements could be compared; in section 5 we include results for turbulence spectra that compare the scales captured by the LES and both types of measurement stations.

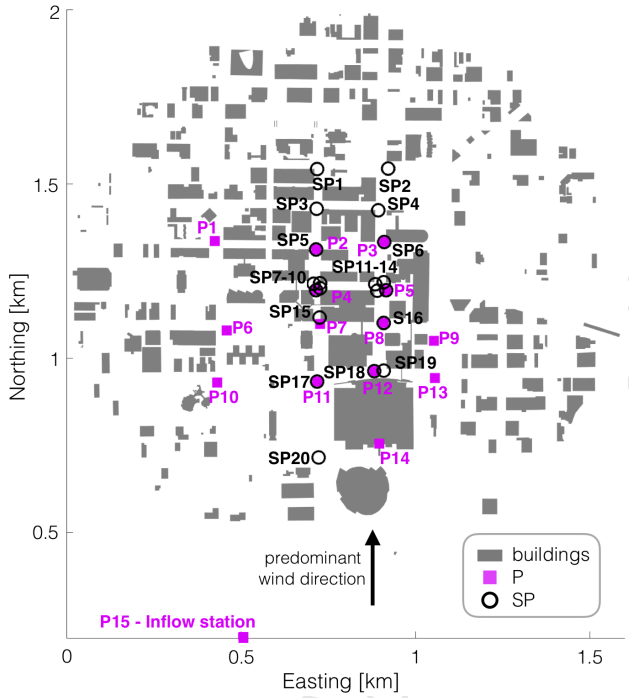

Figure 1: Downtown locations of the portable (P) and super portable (SP) weather display system [19, 18].

3. Summary of computational set-up for the RANS simulation

This section briefly introduces the set-up for the RANS simulation performed with the open source CFD solver OpenFOAM v4.0. A more detailed description of the set-up can be found in [18], where the effect of inflow uncertainties on velocity and concentration predictions in downtown Oklahoma City was quantified for the same 30-minute period of interest used in the present study.

3.1. Governing equations, discretization and solution method

The governing equations are the steady incompressible RANS equations for neutrally stratified flow [16]. The simulations used the k-ε turbulence model, which computes the Reynolds stresses based on a linear eddy viscosity hypothesis [21]. The equations were discretized using the finite-volume method, with second order upwind schemes for velocity, turbulence kinetic energy and turbulence dissipation. The simulations were run until the residuals dropped below 10^{-6} for all variables.

3.2. Computational domain and boundary conditions

The domain size was defined based on the COST action 732 best practice guidelines [22], considering the full range of wind direction simulated for the UQ study ($70° - 120°$). Depending on the specific wind direction of a simulation, the side boundaries are defined as either inlets or outlets (Figure 2a).

Zero-gradient boundary conditions are imposed at the outlets, while fully developed neutral surface layer profiles [23] are defined at the inlets for the velocity (U), the turbulence kinetic energy (k), and the dissipation rate (ε):

$$U = \frac{u_*}{\kappa} ln\left(\frac{z + z_0}{z_0}\right), \quad k = \frac{u_*^2}{\sqrt{C_\mu}}, \quad \varepsilon = \frac{u_*^3}{\kappa\,(z + z_0)}. \tag{1}$$

κ is the von Karman constant(0.41), and C_μ a turbulence model constant (0.09). The friction velocity u_* is computed from the specified aerodynamic roughness z_0, and the reference velocity measured at 30m height(z) at P15. At the top boundary a constant shear stress boundary condition is applied by specifying the velocity, turbulence kinetic energy and dissipation rate as the values given by the inlet profiles at the height of the top boundary.

The computational mesh, shown in Figure 2b consisted of 7.4 million cells; a mesh dependence study has been presented in [18].

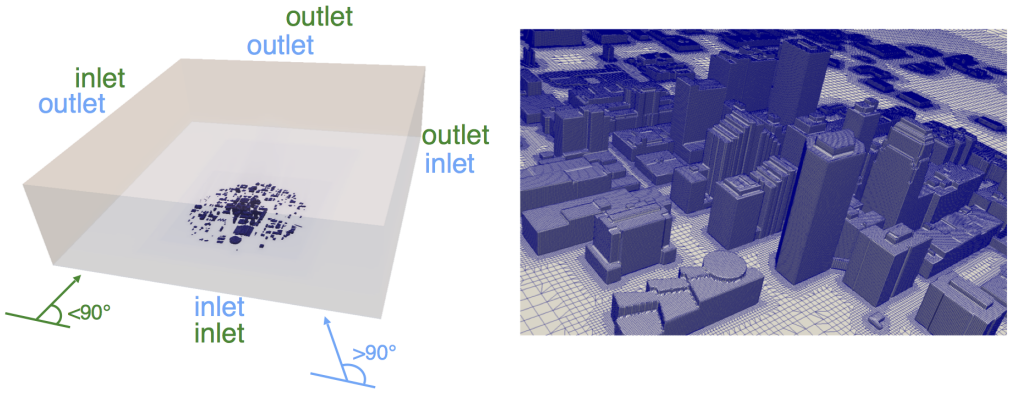

(a) (b)

Figure 2: RANS computational domain (a) and mesh view (b)[18].

3.3. UQ analysis

The study included an investigation of the effect of uncertainty in the inflow boundary conditions. We defined three uncertain parameters: the velocity magnitude (U), direction (θ), and roughness length (z_0). Probability distributions for these uncertain parameters were defined based on the available measurements at the inflow station (P15).

A non-intrusive polynomial chaos expansion approach [24] was used to propagate the uncertainties to the quantities of interest, i.e. the velocity and concentration at the different measurement stations. The integrals defining the Fourier coefficients were calculated using tensor grid quadrature. We used 9 points for each uncertain parameter, leading to a total of 729 RANS simulations.

4. Computational set-up for the LES simulation

The LES simulations were also performed with the open source CFD solver OpenFOAM v4.0. The following sections present the governing equations and the computational set-up for the LES, identifying the main differences with the RANS set-up.

4.1. Governing equations

LES relies on applying a filtering operation which decomposes the instantaneous fields into filtered, $\widetilde{\langle\,\rangle}$, and subgrid scale, $\langle\,\rangle'$, components: $u(x,t) = \widetilde{u}(x,t) + u'(x,t)$; $p(x,t) = \widetilde{p}(x,t) + p'(x,t)$. This leads to the following set of governing equations for a neutrally stratified surface layer flow:

$$\frac{\partial \widetilde{u_i}}{\partial x_i} = 0, \tag{2}$$

$$\frac{\partial \widetilde{u_i}}{\partial t} + \widetilde{u_j}\frac{\partial \widetilde{u_i}}{\partial x_j} = -\frac{1}{\rho}\frac{\partial \widetilde{p}}{\partial x_i} + \nu\frac{\partial^2 \widetilde{u_i}}{\partial x_j^2} - \frac{\partial \tau_{ij}}{\partial x_j}, \tag{3}$$

where the large scales of motion are resolved explicitly, while the small scales, represented by the subgrid stress tensor, τ_{ij}, are parametrized through the subgrid scale (SGS) model. Thus, the SGS model represents the only source of turbulence modeling errors [25]. We use the Smagorinsky SGS model [26, 27], which employs a linear eddy-viscosity model to relate the SGS stress to the filtered rate of strain:

$$\tau_{ij} = -2\nu_T \widetilde{S_{ij}}, \tag{4}$$

where, ν_T is the eddy-viscosity coefficient, and $\widetilde{S_{ij}} = 0.5\left(\frac{\partial \widetilde{u_i}}{\partial x_j} + \frac{\partial \widetilde{u_j}}{\partial x_i}\right)$.

In the Smagoringsky model the eddy-viscosity coefficient is computed as:

$$\nu_T = l_S^2 \overline{S} = (C_S \Delta)^2 \overline{S} \tag{5}$$

where $\overline{S}$ is the characteristic filtered rate of strain, l_S is the Smagorinsky length scale, which is proportional to the filter width Δ through the Smagorinsky coefficient, C_S. The implicit filter selected in OpenFOAM uses $\Delta = V_c^{1/3}$, where V_c corresponds to the volume of the cells [28]. The Smagorinsky constant, C_S, is set to its original value of 0.167 [26, 27]. We note that a variety of more advanced subgrid scale models are available in OpenFOAM, but these were found to reduce stability of the simulations. In addition, previous work on arrays of cubes has shown that the Smagorinsky model produces satisfactory results for urban canopy flows [29, 4].

4.2. Computational Domain and Mesh

The geometry is identical to the one used for the RANS UQ study [18], but the size of the domain is slightly reduced to save computational time and resources. The RANS domain was set-up to run simulations with different inflow wind directions, hence the domain size allowed the sides to become inlet or outlets. The reduced LES domain size was designed to respect the best practice guidelines for urban flows [22] for the simulated wind direction of 97.86°. The domain covers approximately 3km by 3km in the horizontal directions, and 900m in the vertical direction. Defining the region of interest as downtown Oklahoma City, the lateral and inflow boundaries are located at a distance larger than $5H_{max}$, while the top height is located at $5H_{max}$ from the tallest building. The outflow boundary condition is located at $11H_{max}$ from the center of the downtown area.

The parallel mesh tool SnappyHexMesh was used to build the computational grid [28]. The mesh is designed to balance resolving part of the inertial subrange of the turbulence spectrum in the region of interest against the computational cost. Different refinement areas were specified to allow a progressive increase of the cell resolution towards the downtown area. Figure 3 depicts the different refinement areas, while Table 2 includes additional details on the mesh resolution. The resolution in the downtown area follows available recommendations: the vertical resolution places approximately 6 mesh points within the first 2m from the ground [30], while the horizontal resolution ensures that the number of grid points across all buildings is larger than 6-8 [3]. The resulting mesh consists of 87.4 million cells; the near-wall resolution results in y+ values within the logarithmic layer, with minimal values down to 30.

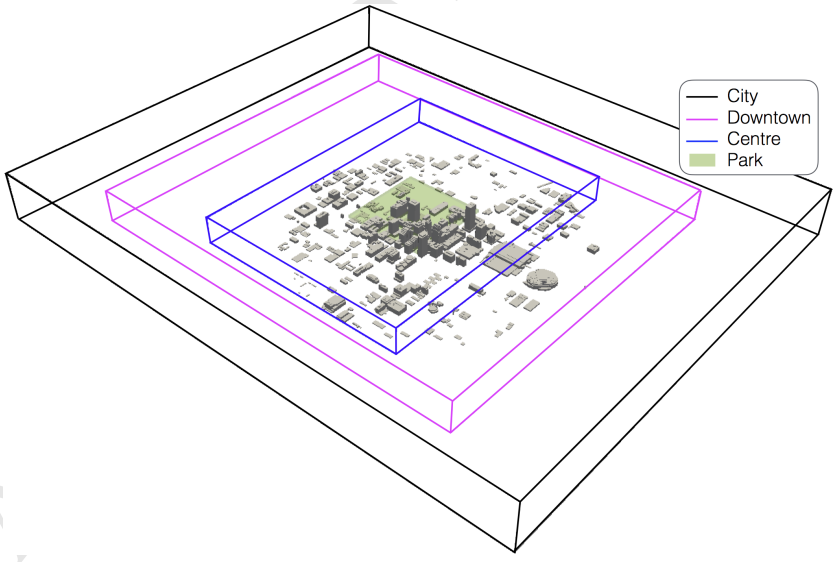

Figure 3: Mesh design composed of 4 refinement areas: city, downtown, center, and park.

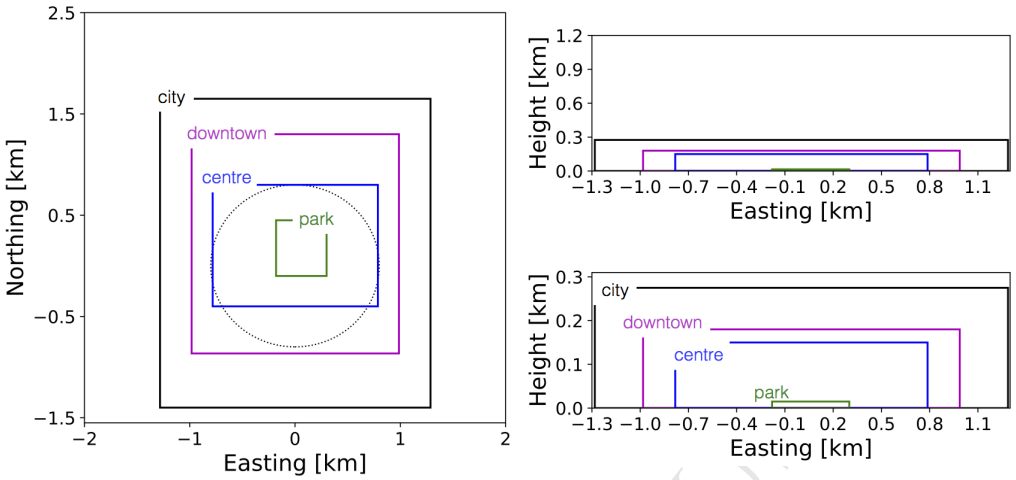

(a) (b)

Figure 4: 2D sketch of the mesh design in the LES simulation: (a) top view, (b) side view and side view detail.

Total number of cells	$87.4 \cdot 10^6$			
BlockMesh number of cells [xyz]	140 x 160 x 100			
Refinement zone names	City	Downtown	Centre	Park
Refinement level	1	2	3	5
$\Delta x[m]$	9.17	4.58	2.29	0.59
$\Delta y[m]$	9.53	4.75	2.38	0.57
$\Delta z[m]$	4.5	2.25	1.12	0.28

Table 2: Mesh design details.

4.3. Boundary Conditions

At the inflow boundary we use the digital filter developed by Xie and Castro [31] to specify an unsteady ABL flow with turbulence structures that are coherent in space and time. The method uses a 2D digital filter on a random field to generate a signal with an exponential correlation function in space and time. It requires inputs for the mean velocity and Reynolds stress profiles, and for three Lagrangian time scales. It has has been used extensively for urban canopy flow simulations, and satisfactory results were reported when comparing LES simulations to wind tunnel experiments for urban test cases [4, 32, 33]. In those cases, the controlled wind tunnel environment provided sufficient data to accurately define the input parameters. This is more challenging in the present study, where limited data for the characterization of the inflow ABL is available.

For the mean velocity profile, we impose a logarithmic neutral surface layer profile. The roughness height is set to 0.29m, corresponding to suburban terrain upstream of the area of interest. The friction velocity is obtained from the reference velocity measured at 30m height at P15, since winds were predominantly from the south and P15 is the south-most station.

Since the 10 second averaged velocity signal from P15 does not provide an accurate estimate for the Reynolds stresses, the stress profiles were specified following boundary layer similarity theory [34]. Based on the velocity scale $u_L = \kappa z(\partial U/\partial z)$ and assuming that $\overline{w'^2} = \overline{u'v'}$, we calculate the profiles as follows:

$$\frac{\overline{u'^2} + \overline{v'^2}}{u_L^2} = 8.5 \quad ; \quad \overline{u'^2} = 2/3(8.5u_L^2) \quad ; \quad \overline{w'^2} = \overline{u'v'} = 2.5u_L^2 \qquad (6)$$

The Lagrangian time scale for the stream-wise velocity was estimated based on the measurement data, since it is expected to be larger than the averaging time used at P15. The integral of the auto-correlation of the stream-wise velocity component corresponded to $\tau_u = 18.29s$, and was converted to a length-scale, $L_u = 110m$, using Taylor's frozen turbulence hypothesis. The corresponding τ_v and τ_w were calculated using the following relationships, which are commonly applied in wind tunnel experiments:

$$L_v = 0.2L_u \quad ; \quad L_w = 0.3L_u \tag{7}$$

The approximations used to define the Reynolds stresses and length scales introduce additional uncertainty in the definition of the inflow boundary conditions in LES. However, this uncertainty can be expected to mainly affect the results in the most upstream part of the domain. When moving downstream into the downtown area of interest, the influence of the turbulence characteristics imposed at the inflow is likely to decrease; in this region the local turbulence characteristics will primarily be governed by the upstream urban geometry.

At the west, east, and top boundaries, symmetry conditions were applied, corresponding to a slip, or shear-stress free, boundary condition. Since the lateral boundaries are far from the downtown area of interest, the definition of these boundary conditions is not expected to influence the results. The outlet is set-up as a zero-gradient boundary condition. Wall functions were used since the high Reynolds number of urban canopy flows does not allow to resolve the laminar sublayer near the walls. At the ground boundaries, a rough wall function for a neutral ABL flow is applied, while on the building surfaces a smooth wall function was used. It is noted that more advanced wall

functions exist (e.g. [35]), but they are not readily available in OpenFOAM, and [29, 4] found satisfactory performance of the logarithmic wall functions when used for urban canopy flows.

4.4. Numerical settings

Second order schemes were applied for the discretization of the velocity gradients. The simulation was run with a time step of 0.02s for a total time of 1854s = $51\tau_{LES}$, where τ_{LES} is the the flow-through time scale based on the largest streamwise building dimension of 222m, and the velocity at 30m height. Statistics were computed over a time-period of $30\tau_{LES}$, after an initialization period of $21\tau_{LES}$. The resulting LES required approximately 340.000 CPU hours on the Stampede cluster, which was built using Xeon E5-2680 8-core Sandy Bridge processors [36].

5. Results

The analysis of the results focuses primarily on comparing the LES to the field measurement data and the nominal RANS simulation presented in [18]. The main objective is to evaluate the predictive capabilities of high-fidelity LES compared to traditional RANS simulations, when used in a deterministic framework that does not account for uncertainties in the boundary conditions or geometrical characterization. The LES results are first evaluated qualitatively using flow field visualizations to reveal the level of detail resolved in the turbulence flow field. Subsequently, we compare the mean wind and turbulence kinetic energy fields from the LES and RANS simulation to the field measurement data recorded during the period of interest.

5.1. Flow field visualization

Figure 5 presents instantaneous contours for the velocity magnitude on a horizontal plane at 8m height and a vertical plane through the center of the domain. The contours show how the flow impacts the buildings, generating recirculation areas with large-scale unsteady structures in the wakes of the geometries. In the vertical direction, the velocity magnitude increases, following the logarithmic profile for the mean velocity imposed at the inlet.

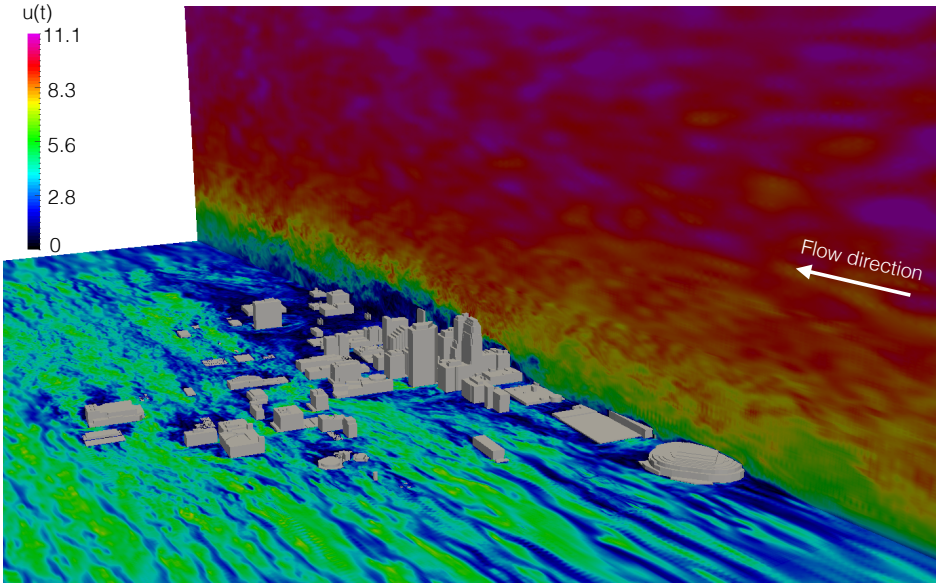

Figure 5: Instantaneous contours for velocity magnitude for planes at 8m height above ground level (z=8m) and at the center of the domain (y=0m).

The Q-criterion, or second invariant of the velocity, ∇U, was computed following equation 8,

$$Q = \frac{1}{2}\left(||\Omega||^2 - ||S||^2\right) \tag{8}$$

where S and Ω are the symmetric and antisymmetric components of ∇U.

Consequently, Q defines the local balance between shear strain rate and vorticity magnitude. Figure 6 shows iso-surfaces of the Q-criterion above 20m height in the downtown area colored by velocity magnitude. The iso-surfaces were generated for $Q = 0.35\text{s}^{-2}$, hence revealing structures where the vorticity magnitude is larger than the shear strain rate. The structures mainly appear near the sharp building edges and in the building wakes, generally exhibiting an increasing velocity magnitude with height. Close to the ground, the velocity is small and the structures are smaller in size.

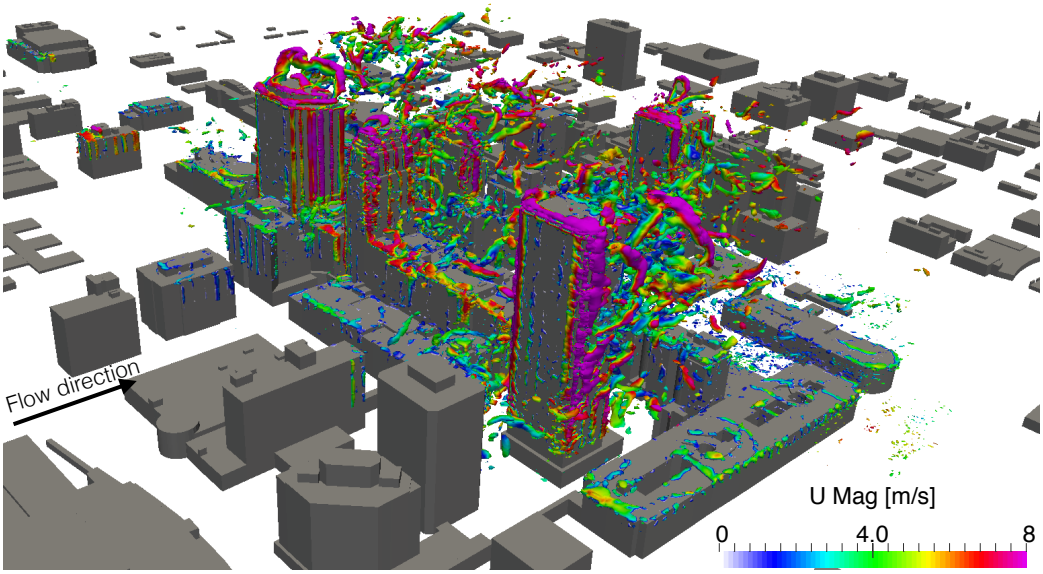

Figure 6: Q contours ($Q = 0.35\text{s}^{-2}$) colored by velocity magnitude in downtown Oklahoma City.

5.2. Comparison of time-averaged velocity field

Figure 7 shows contour plots for the time-averaged velocity magnitude at 8m height from the LES and RANS predictions. The plot shows very similar

patterns for the velocity field around the buildings, with relatively small local differences at specific locations in the city. For example, on the west side of the building indicated by number 1, we can observe a wider region with reduced velocities in the LES. In locations 2 and 3, the LES predicts higher wind speeds through the corridors parallel to the wind direction.

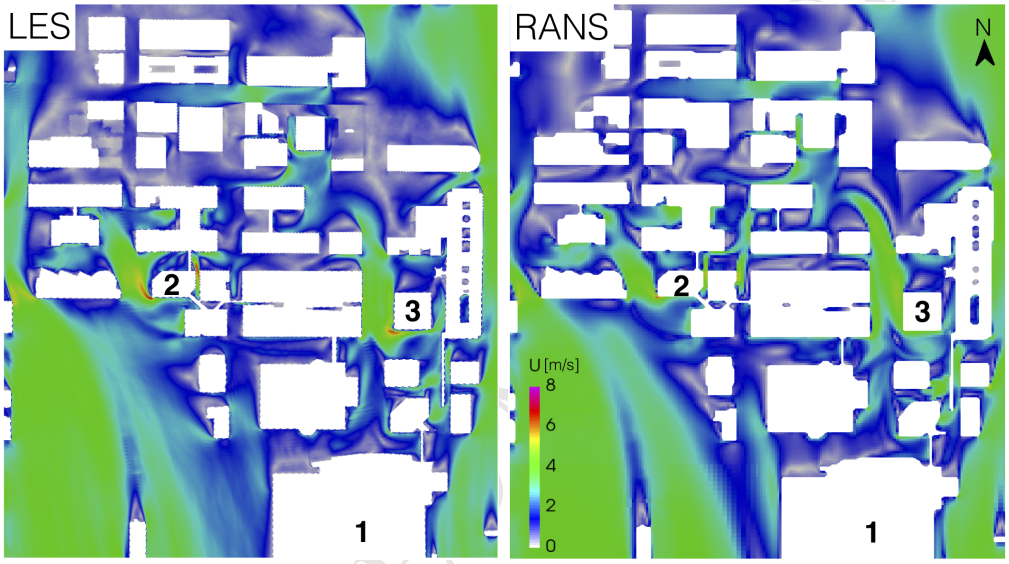

(a) (b)

Figure 7: Time-averaged velocity contours at 8m height from the LES and RANS simulations. N: north orientation.

The differences between both results in the downtown area are highlighted in figure 8, using contour plots of the relative difference in the local velocity magnitude and the absolute difference in the local wind direction. Generally, good agreement between the LES and RANS results is obtained, except in localized areas where the LES predicts a stronger acceleration compared to the RANS simulation. For the wind direction, larger differences are observed

in the building wakes, where recirculation areas are present. Some of the locations with larger discrepancies, such as P2, P3 or P12, correspond to P stations where large turbulence model form uncertainty has been observed previously [17]. Consequently, RANS simulations are unlikely to correctly predict the flow behavior in these locations.

We note that in the most upstream parts of the domain, larger differences are observed in the velocity magnitude predicted by the LES and RANS than observed in figure 8. These differences are mainly attributed to the fact that the required averaging time for the unperturbed ABL, which has a large streamwise length scale, is longer than for the flow in the downtown area.

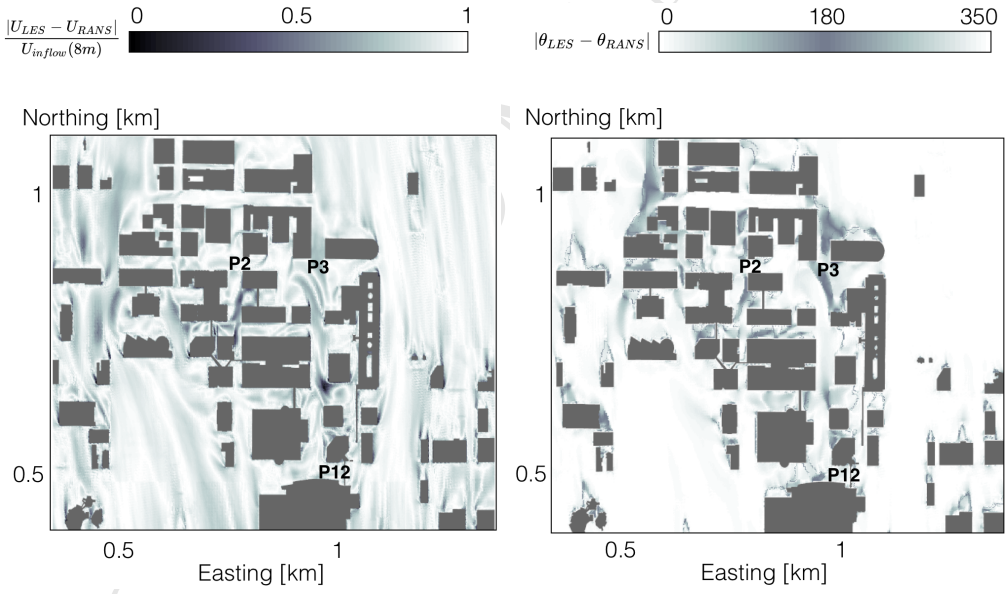

Figure 8: Contours of the relative difference in velocity magnitude (U) and absolute difference in velocity direction (θ) between the LES and RANS results at 8m height.

Figures 9, 10 and 11 compare the discrepancies between the simulation

results and the field measurement data for the time-averaged velocity. In figures 9 and 10, the differences for the velocity magnitude and direction at all P and SP locations are plotted. The line indicates zero discrepancy from the experimental data; points located above the line indicate an over-prediction, while points below the line indicate an under-prediction with respect to the measurements. For the velocity magnitude 17 points show a larger discrepancy in RANS, in the remaining 17 points the LES discrepancy is larger. These numbers indicate an overall comparable performance between both methods, although it should be noted that the RANS discrepancies are significantly larger in 6 out of 34 points, while for the LES this only occurs in 1 point. The results do not reveal a dominant over- or under-prediction. The velocity direction also shows similar performance between both models, the scatter in the data is smaller than for the velocity magnitude implying a closer agreement in the wind direction predicted by RANS and LES. The models generally seem to predict a wind direction that is rotated counterclockwise compared to the experimentally measured data.

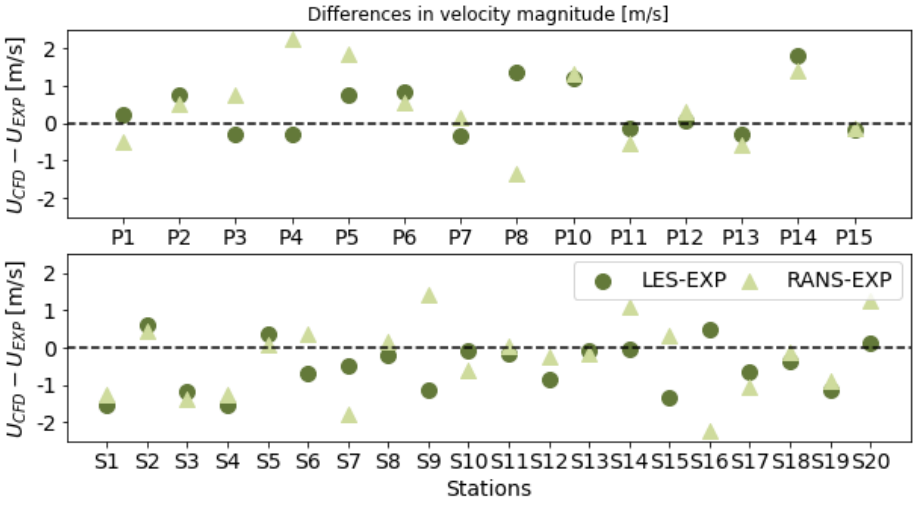

Figure 9: Scatter plot of the discrepancies in velocity magnitude from the LES and the experiment and from the RANS and the experiment at the field measurement sensors.

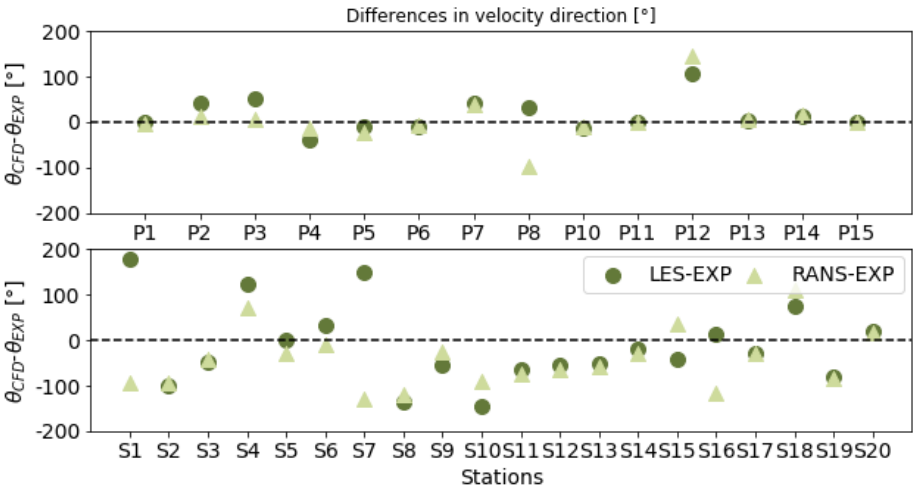

Figure 10: Scatter plot of the discrepancies in velocity direction from the LES and the experiment and from the RANS and the experiment at the field measurement sensors.

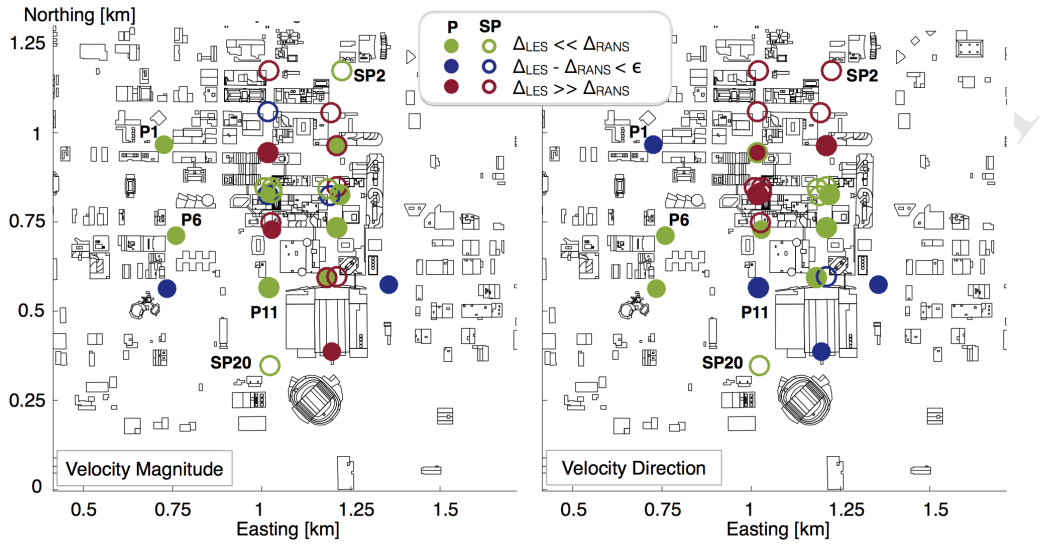

Figure 11: Comparison of LES and RANS model performance for predicting the velocity magnitude and direction measured during the field experiment. Full marker: P stations; marker: SP stations.

Figure 11 visualizes spatial variation in the model performance comparison by classifying the prediction at each measurement station using: (1) $|\Delta_{LES}| << |\Delta_{RANS}|$, hence LES outperforms RANS; (2) $||\Delta_{LES}| - |\Delta_{RANS}|| \leq \epsilon$, where ϵ is $0.1\%U_{exp}$ or 5^o, hence LES and RANS are comparable ; (3) $|\Delta_{RANS}| << |\Delta_{LES}|$, hence RANS outperforms LES. The plot shows how the velocity magnitude prediction using LES is better in stations located at the outskirts of the downtown area, such as P1, P6, P11, SP2 or SP20. For the velocity direction, the LES results show consistent improvements at the south most sensor locations. In the center of the downtown area the model performance is highly variable.

These results demonstrate that the application of high-fidelity LES to resolve the mean flow does not consistently guarantee a better prediction of

flow measurements in complex urban canopy geometries. An interesting observation is that the areas where the predictions deviate more strongly from the experimental results correspond to the locations with larger uncertainty identified in previous uncertainty quantification studies [16, 18]. In these stations the results are highly sensitive to variability in the inflow conditions, and simulation results with low turbulence model uncertainty can therefore still deviate considerably from the experimental data. The resulting improvement in the agreement with the experimental data is small compared to the RANS simulation, and comes at a considerable increase in computational cost.

5.3. Comparison of turbulence kinetic energy field and velocity spectra

Figure 12 shows contour plots for the turbulence kinetic energy at 8m height from the LES and RANS predictions. The RANS simulation qualitatively indicates locations where the turbulence kinetic energy increases, but it predicts a lower turbulence kinetic energy in all areas compared to the LES simulation. We note that the time statistics for the turbulence kinetic energy at the available SP stations were converged, but the results in the upstream part of the domain again indicate that the required averaging time for regions with relatively unperturbed ABL flow might be longer than for the flow in the downtown area.

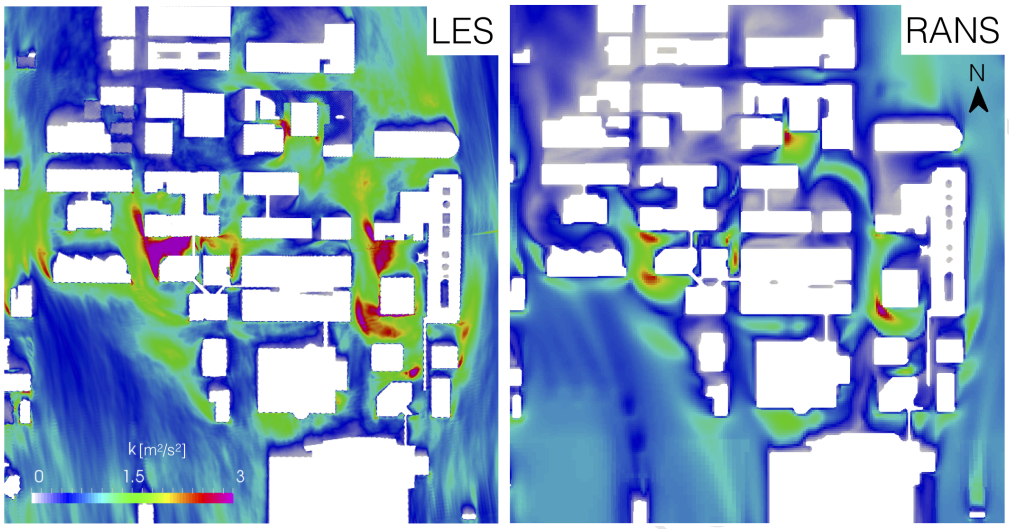

(a) (b)

Figure 12: Time-averaged turbulence kinetic energy contours at 8m height from the LES and RANS simulations. N: north orientation.

Figures 13 and 14 compare the discrepancies between the simulation results and the field measurement data for the turbulence kinetic energy. We only consider the SP sensors, since the 10 second averaged measurement from the P sensors would underestimate the turbulence kinetic energy. Figure 13 shows a scatter plot of the discrepancies between the simulation results and the experimental mean at the stations. The plot clearly demonstrates the superior performance of the LES for predicting the turbulence kinetic energy: the LES value is closer to the measurement in 80% of the points. Both the RANS and LES results consistently underestimate the value of the turbulence kinetic energy.

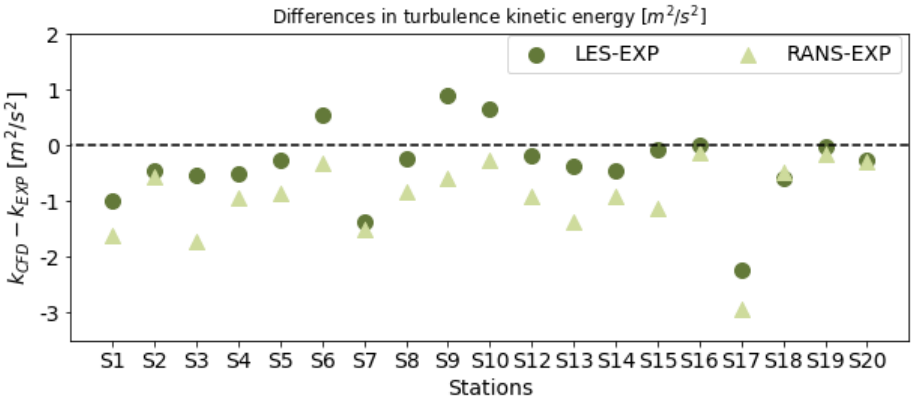

Figure 13: Scatter plot of the discrepancies in turbulence kinetic energy from the LES and the experiment and from the RANS and the experiment at the field measurement sensors SP.

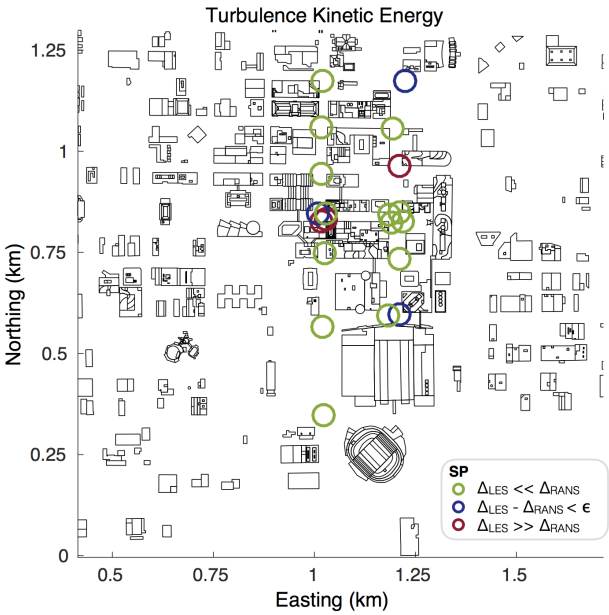

Figure 14: Comparison of LES and RANS model performance for predicting the turbulence kinetic energy measured during the field experiment. Full marker: P stations; marker: SP stations.

Figure 14 visualizes spatial variation in the model performance comparison by classifying the prediction as in Figure 11. The plot confirms that improved predictions for the turbulence kinetic energy can be obtained with LES throughout the urban canopy geometry.

To further analyze the turbulence predicted by the LES, figure 15 presents power spectral densities for the streamwise velocity component at four different locations in Oklahoma City. In the LES, the areas around stations 1 and 4 have a lower mesh resolution than those around stations 2 and 3, which are closer to the downtown area of interest. This is reflected in the fact that the energy content at stations 1 and 4 decays at smaller frequencies than at stations 2 and 3. Locations 2, 3 and 4 show both P and SP measurements, indicating the effect of the 10 second averaging in the P data. At lower frequencies, all plots show good agreement between the experiments and the simulations, which proves that the numerical approach can produce the same intensity of turbulence fluctuations measured by the wind anemometers. All measurements and numerical results exhibit the $-5/3$ slope in the inertial subrange, where energy is transfered from the larger eddies in the production range to the smaller eddies in the viscous dissipation range.

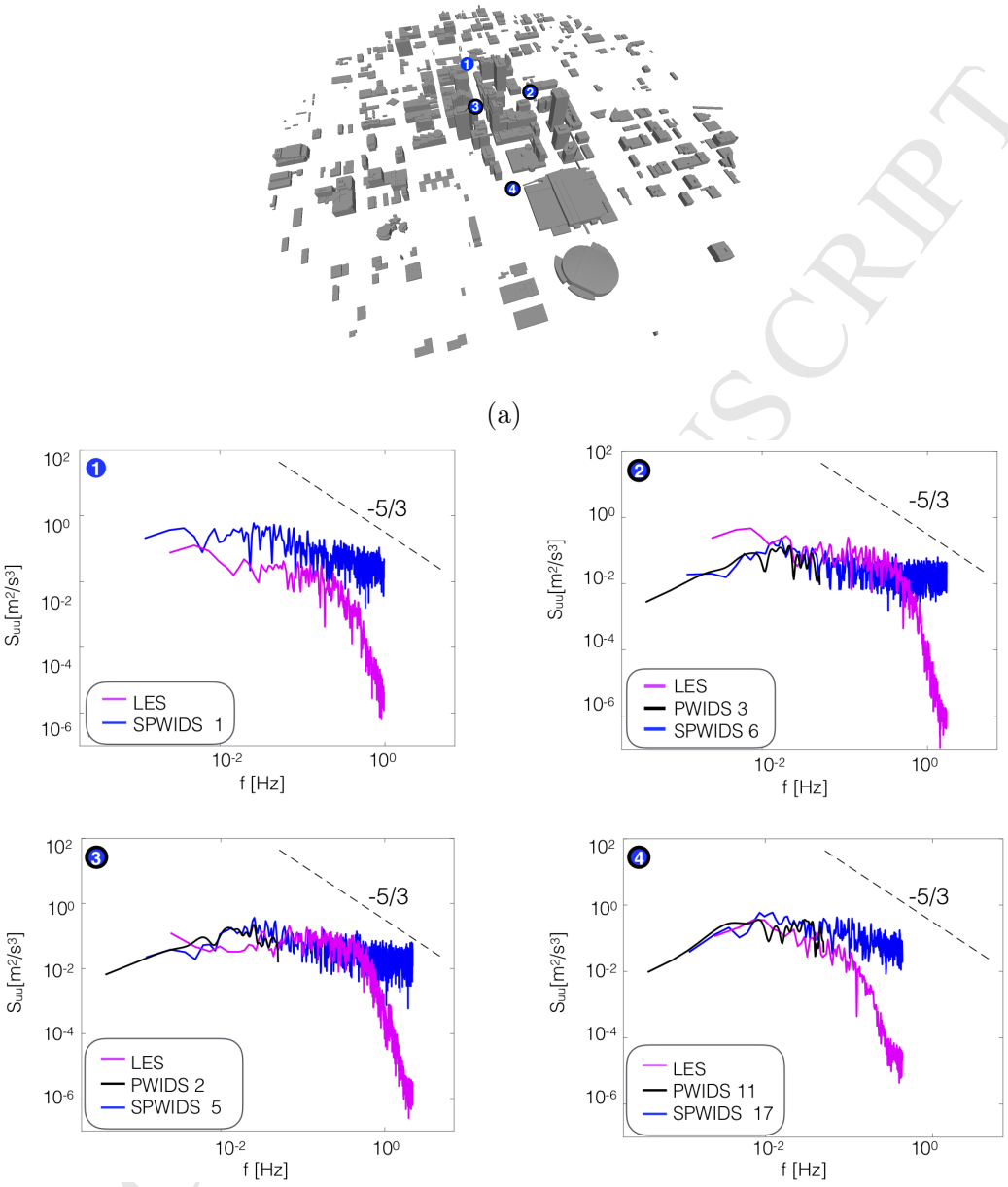

Figure 15: (a) locations in the downtown area where the spectra are calculated, (b) corresponding power spectral density plots: 1) north, SP1; 2) east, P3 and SP6; 3) west, P2 and SP5; 4) south, P11, SP17.

In summary, we can conclude that the turbulence spectra produced by the inflow generator and the building geometries is very realistic compared to the measurements. The large eddy simulation results predict a similar range of scales and corresponding energy content as the experimental data.

5.4. Comparison of LES time-averaged result with previous uncertainty quantification study

In order to further assess the predictive capabilities of the current LES approach, we compare the mean LES wind predictions with a previous RANS inflow UQ study performed for the same period of interest, summarized in section 3 and published in [18].

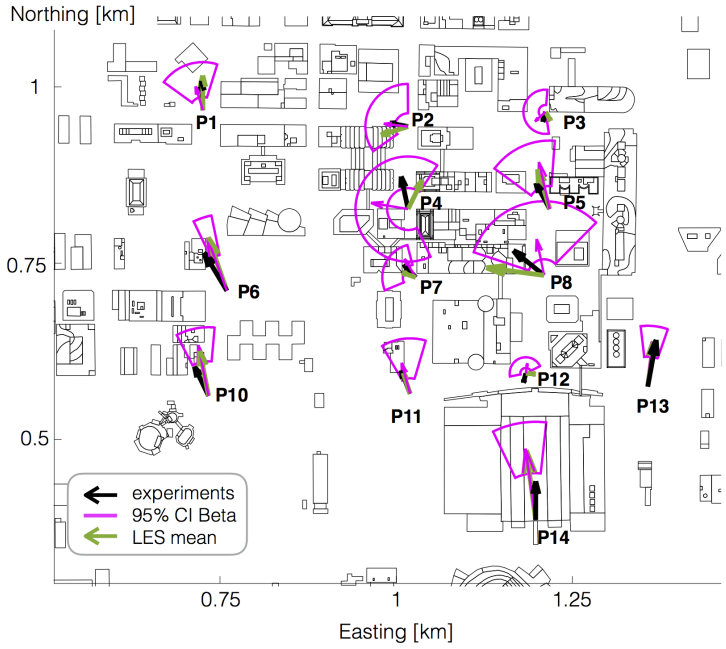

Figure 16: Comparison between experimental data, LES time-averaged velocity and UQ study results for the wind prediction at the P stations [18]. Black: experiments, magenta: uncertainty quantification: green: LES.

Figure 16 presents the results at 13 P stations in the downtown area. The black arrows show the velocity vectors from the field measurements, time-averaged over the experimental period of interest. The green arrows represent the mean velocity predicted by the LES at the stations, while the magenta arrows show the mean from the UQ study. The magenta arcs represent the 95% confidence intervals for the predicted velocities, which are calculated as the values where the cumulative density function is 0.025 and 0.975. The 95% CI of the velocity magnitude is represented by the radii of the annulus, while the 95% CI for the wind direction is represented by the sector angle.

In stations where the inflow uncertainty has limited influence such as P6, P10, P13 or P14 it can be observed how the LES mean prediction is close to the RANS results and the field measurement. However, in stations that are highly sensitive to changes in the inflow boundary conditions, such as P3, P4, P8 or P12, both the LES and RANS simulations have difficulties to predict the experimental value. This suggests that UQ studies will also be required to improve the predictive capabilities of higher fidelity simulation approaches such as LES.

6. Conclusions

The objective of this study was to compare urban flow predictions obtained using RANS and LES to field measurements, and interpret the results to identify outstanding challenges in LES simulations of urban flows.

The LES simulations were carefully designed to have a grid resolution that resolves the turbulence down to the inertial subrange in the downtown area of interest, and they used an inflow boundary condition that gener-

ates turbulence representative of an ABL flow. The results show negligible improvement in the LES prediction of the mean velocity field compared to the RANS result, improving the wind flow predictions in only 17 out of 34 stations. In contrast, there is a clear improvement in the prediction of the turbulence kinetic energy: the LES outperforms the RANS simulation in 80% of the available measurement locations. In addition, the LES produces turbulence spectra that are in good agreement with the measurements regarding the scales and energy content of the turbulence.

This study highlights the need for further validation of numerical simulations with field measurements that represent the full complexity of urban flows. While LES is an essential tool to improve our understanding of flow patterns in complex configurations, there are considerable challenges when predicting field measurements of urban flow. In particular, it was found that the locations where LES does not provide a better prediction of the mean velocity field than RANS, correspond to the locations where the RANS results are highly sensitive to the inflow boundary condition. This suggests that a higher-fidelity turbulence model does not guarantee a better prediction of the flow in areas with large uncertainty related to the inflow boundary condition. Hence, there are significant opportunities to improve the predictive capabilities of LES for urban flows by using the simulations in a UQ framework that can reflect the influence of these uncertainties on the results. Currently, the considerable computational cost of LES makes such UQ studies, which can require hundreds of simulations, intractable. In this respect, multi-fidelity simulation strategies for uncertainty quantification are a promising alternative to explore: improved predictive capabilities could likely be obtained

using a small number of high-fidelity LES simulations to complement a large number of low-fidelity RANS model results [37].

Acknowledgments

The first author's contribution to this work was supported by the doctoral (PhD) grant number 131423 for strategic basic research from the Agency for Innovation by Science and Technology in Flanders (IWT). This work used the Extreme Science and Engineering Discovery Environment (XSEDE), which is supported by National Science Foundation grant number CTS160009 [36].

[1] United Nations, World's population increasingly urban with more than half living in urban areas (January 2016).
URL http://www.un.org/en/development/desa/news/population/world-urbanization-prospects-2014.html

[2] Chang, C. and Meroney, R.N., Concentration and flow distributions in urban street canyons: wind tunnel and computational data, Journal of Wind Engineering and Industrial Aerodynamics 91 (9) (2003) 1141 – 1154. doi:https://doi.org/10.1016/S0167-6105(03)00056-4.

[3] Tseng, Y.H., Meneveau, C. and Parlange, M.B., Modeling flow around bluff bodies and predicting Urban Dispersion using large eddy Simulation, Environmental Science & Technology 40 (8) (2006) 2653–2662. doi:10.1021/es051708m.

[4] Xie, Z-T. and Castro, I.P., Large-eddy simulation for flow and dispersion in urban streets, Atmospheric Environment 43 (13) (2009) 2174 – 2185. doi:10.1016/j.atmosenv.2009.01.016.

[5] Santiago, J. L., Dejoan, A., Martilli, A., Martin, F. and Pinelli, A., Comparison Between Large-Eddy Simulation and Reynolds-Averaged Navier–Stokes Computations for the MUST Field Experiment. Part I: Study of the Flow for an Incident Wind Directed Perpendicularly to the Front Array of Containers, Boundary-Layer Meteorology 135 (1) (2010) 109–132. doi:10.1007/s10546-010-9466-3.

[6] Gousseau, P., Blocken, B., Stathopoulos, T., and van Heijst, G.J.F., CFD simulation of near-field pollutant dispersion on a high-resolution grid: A case study by LES and RANS for a building group in downtown Montreal, Atmospheric Environment 45 (2011) 428–438. doi:https://doi.org/10.1016/j.atmosenv.2010.09.065.

[7] Tominaga, Y. and Stathopoulos, T., CFD modeling of pollution dispersion in a street canyon: Comparison between LES and RANS, Journal of Wind Engineering and Industrial Aerodynamics 99 (4) (2011) 340 – 348, the Fifth International Symposium on Computational Wind Engineering. doi:https://doi.org/10.1016/j.jweia.2010.12.005.

[8] Salim, S.M., Cheah, S.C. and Chan, A., Numerical simulation of dispersion in urban street canyons with avenue-like tree plantings: Comparison between RANS and LES, Building and Environment 46 (9) (2011) 1735 – 1746. doi:https://doi.org/10.1016/j.buildenv.2011.01.032.

[9] Hanna, S.R., Brown, M.J., Camelli, F.E., Chan, S.T., Coirier, W.J., Hansen, O.R., Huber, A.H., Kim, S. and Reynolds, R.M., Detailed Simulations of Atmospheric Flow and Dispersion in Downtown Manhattan:

An Application of Five Computational Fluid Dynamics Models, Bulletin of the American Meteorological Society 87 (12) (2006) 1713–1726. doi:10.1175/BAMS-87-12-1713.

[10] Patnaik G., Boris J.P., Young T.R. and Grinstein F.F., Large Scale Urban Contaminant Transport Simulations With Miles, ASME Journal of Fluids Engineering 129 (12). doi:10.1115/1.2801368.

[11] Dejoan, A., Santiago, J.L., Martilli, A., Martin, F. and Pinelli, A., Comparison between large-eddy simulation and Reynolds-averaged Navier-Stokes computations for the MUST field experiment. Part II: effects of incident wind angle deviation on the mean flow and plume dispersion, Boundary-Layer Meteorology 135 (1) (2010) 133–150. doi:10.1007/s10546-010-9467-2.

[12] Neophytou, M., Gowardhan, A. and Brown, M., An inter-comparison of three urban wind models using Oklahoma City Joint Urban 2003 wind field measurements, Journal of Wind Engineering and Industrial Aerodynamics 99 (2011) 357–368. doi:https://doi.org/10.1016/j.jweia.2011.01.010.

[13] Harms, F., Leitl, B., Schatzmann, M. and Patnaik, G., Validating LES-based flow and dispersion models, Journal of Wind Engineering and Industrial Aerodynamics 90 (2011) 289–295. doi:https://doi.org/10.1016/j.jweia.2011.01.007.

[14] Nakayama, H., Takemi, T. and Nagai, H., Large-eddy simulation of urban boundary-layer flows by generating turbulent inflows from mesoscale

meteorological simulations, Atmospheric Science Letters 13 (3) (2012) 180–186. doi:10.1002/asl.377.

[15] Biltoft, C.A., Customer report for Mock urban Setting test, Tech. Rep. WDTC-FR-01-121, Army Dugway Proving Ground, Dugway, UT. (2001).

[16] García-Sánchez, C., Philips, D.A. and Gorlé, C., Quantifying inflow uncertainties for CFD simulations of the flow in downtown Oklahoma City, Building and Environment 78 (118-129). doi:https://doi.org/10.1016/j.buildenv.2014.04.013.

[17] Gorlé, C., García-Sánchez, C. and Iaccarino, G., Quantifying inflow and RANS turbulence model form uncertainties for wind engineering flows, Journal of Wind Engineering and Industrial Aerodynamics 144 (2015) 202–212. doi:https://doi.org/10.1016/j.jweia.2015.03.025.

[18] García-Sánchez, C., Van Tendeloo, G. and Gorlé, C., Quantifying inflow uncertainties in RANS simulations of urban pollutant dispersion, Atmospheric Environment 161 (2017) 263–273. doi:https://doi.org/10.1016/j.atmosenv.2017.04.019.

[19] Allwine, K.J. and Flaherty, J.E., Joint Urban 2003: Study Overview and Instrument Locations, PR 15967, PNNL (2006).

[20] R.M. Young website, http://www.rmyoungusa.com (2018).

[21] Wilcox, D.C., Turbulence Modeling for CFD, La Cañada: DCW Industries Inc., 1993.

[22] Franke, J., Hellsten, A., Schlünzen, H. and Carissimo, B., Best practice guideline for the CFD simulation of flows in the urban environment, Tech. rep., COST Action 732 (May 2007).

[23] Richards, P.J. and Hoxey, R.P., Appropriate boundary conditions for computational wind engineering models using the k-ε turbulence model, Journal of Wind Engineering and Industrial Aerodynamics 46-47 (1993) 145–153. doi:https://doi.org/10.1016/j.jweia.2010.12.008.

[24] Iaccarino, G., Introduction to uncertainty representation and propagation, AVT-193 short course on uncertainty quantification, Tech. rep., NATO Research and Technology Organization, Neuilly-sur-Seine (2011).

[25] Kosović, B., Subgrid-scale modelling for the large-eddy simulation of high-Reynolds-number boundary layers, Journal of Fluid Mechanics 336 (1997) 151–182. doi:10.1017/S0022112096004697.

[26] Smagorinsky, J., General circulation experiments with the primitive equations, Monthly Weather Review 91 (3) (1963) 99–164. doi:10.1175/1520-0493(1963).

[27] Lilly, D. K., The representation of small scale turbulence in numerical simulation experimentsdoi:https://doi.org/10.1063/1.858280.

[28] Greenshields, C.J., CFD Direct Ltd., Openfoam user guide, Tech. rep., OpenFOAM Foundation Ltd. (2011-2016).

[29] Xie, Z.-T. and Castro, I.P., LES and RANS for turbulent flow over arrays of wall-mounted cubes, Flow, Turbulence and Combustion 76 (3) (2006) 291–312. doi:10.1007/s10494-006-9018-6.

[30] Tominaga, Y., Mochida, A., Yoshie, R., Kataoka, H., Nozu, T., Yoshikawa, M. and Shirasawa, T., AIJ guidelines for practical applications of CFD to pedestrian wind environment around buildings, Journal of Wind Engineering and Industrial Aerodynamics 96 (10) (2008) 1749 – 1761, 4th International Symposium on Computational Wind Engineering (CWE2006). doi:https://doi.org/10.1016/j.jweia.2008.02.058.

[31] Xie, Z.-T. and Castro, I.P., Efficient generation of inflow conditions for large eddy simulation of street-scale flows, Flow, Turbulence and Combustion 81 (3) (2008) 449–470. doi:10.1007/s10494-008-9151-5.

[32] Castro, I.P. and Xie, Z.-T., LES for modeling the urban environment, Physics of Fluids 78 (2009) 4–10.
URL https://eprints.soton.ac.uk/148061/

[33] Kim, Y., Castro, I.P. and Xie, Z.-T., Divergence-free turbulence inflow conditions for large-eddy simulations with incompressible flow solvers Computers and Fluids, Computers & Fluids 84 (2013) 56–68.

[34] Stull, R.B., An introduction to boundary layer meteorology, Springer Netherlands, 1988.

[35] Larsson,J., Kawai, S., Bodart, J. and Bermejo-Moreno, I., Large eddy simulation with modeled wall-stress: recent progress and future directions, Mechanical Engineering Reviews 3 (1) (2016) 15–00418–15–00418. doi:10.1299/mer.15-00418.

[36] Towns, J., Cockerill, T., Dahan, M., Foster, I., Gaither, K., Grimshaw, A., Hazlewood, V., Lathrop, S., Lifka, D., Peterson, G.D., Roskies, R., Scott, J.R, Wilkins-Diehr, N., XSEDE: accelerating scientific discovery, Computing in Science & Engineering 16 (2014) 62–74.

[37] Peherstorfer, B. Willcox, K. and Gunzburger, M., Survey of multifidelity methods in uncertainty propagation, interference and optimization, SIAM Review.

- RANS and LES results for the flow in Oklahoma City are compared to field measurements
- LES mean velocity predictions are more accurate in 50% of the measurement stations
- LES turbulence kinetic energy predictions are more accurate in 80% of the stations
- LES mean velocity is less accurate in stations sensitive to inflow variability in RANS
- Accounting for the different uncertainties in urban flow simulations is essential